Nanoprinting Controls for Thin Film Fabrication

A. Haldar[1], J. Richer[3], S. Curran[2]

[1]Department of Physics, Science and Research Bld. 1, University of Houston, Houston, Texas 77204, United States

[2]Department of Physics and Advanced Manufacturing Institute, University of Houston, Houston, Texas 77204, United States

[3]University of Maryland, College Park, Maryland 20742, United States

Abstract

Inkjet technology is increasingly viewed as more than just a printing or marking technique. A detailed overview is presented of the key inkjet developments to elucidate the importance of inkjet technology as a relevant and key industrial technology. The theory describing printing processes at the nanoscale is presented detailing the methodologies and phenomenology involved including pressure waves deposition. The mathematical details are presented, which includes a description of the experimental procedures involved in the deposition process of an inkjet printed film.

Introduction

Historical overview of Inkjet Technology

The first pioneering work in the field of ink-jet printing was performed by Lord Kelvin, who invented the inkjet-like Siphon recorder in 1858. It used a siphon to produce a continuous stream of ink onto a moving paper ribbon, and a driving signal controlled the movement of the siphon. This was used for the automatic recording of telegraph messages and was patented in

1867. The experimental foundation of the modern inkjet technology was attributed to Savart as early as 1833 [1]. He observed the phenomena of uniform drop formation by the break-up of liquid jets issuing from an orifice. He concluded that the liquid jet break-up was governed by physical laws and produced uniform drops using acoustic energy. The mathematical framework was laid by Plateau and Lord Rayleigh [2,3]. Plateau derived the relationship of jet diameter to drop size, and Lord Rayleigh mathematically described the instability of the liquid jets. The role of surface tension was explored by Young in 1804 [4] and Laplace in 1805 [5].

Working devices based on the physical principles of drop formation started being commercially available from the 1950s. The patent of the first practical inkjet device was credited to Elmqvist from the Siemens-Elema company in 1951 and the 'Mingograph' device was released in 1952. In the early 1960s Sweet (Stanford University) demonstrated that by applying a pressure wave pattern to the ink stream, the inkjet issuing from the orifice could be broken into uniform drops [6]. The drops emerge in the presence of an electrostatic field and can be charged selectively. The charged drops are deflected to a predefined location by another electrostatic field and thus, form an image on the substrate. The uncharged drops were captured and re-circulated in the system. This type of system is known as continuous inkjet printing process (CIJ) because drops are continuously produced and their trajectories are varied by the amount of charge applied (US Patent 3,596,275). The first commercial CIJ printing device was Videojet 9600, based on Sweets invention and released by the A.B. Dick Company in 1968.

The CIJ printers possessed complex systems which had to include charging and deflection electrodes, drop capture mechanism and re-circulation systems. These shortcomings were overcome by the drop-on-demand (DOD) printers which created drops only when an actuation pulse was provided. In late 1940s, Hansell invented the first DOD device which used

a piezoelectric disc to create pressure waves used to break-off the ink jet and create drops [7]. However, the groundwork of the modern piezoelectric inkjet (PIJ) printers was laid by three patents in 1970s [8-10]. All of them used a piezoelectric to generate pressure waves in the ink chamber which caused the drop formation. When an electrical driving voltage is applied to the piezoelectric unit that is coupled to the ink, the unit deforms and causes a volumetric change in the fluid. This change generates pressure waves which are used to produce the drop which ejects out of the orifice. Thermal inkjet (TIJ) printers were developed by replacing the piezoelectric by a thermal transducer which could be miniaturized. At present both PIJ and TIJ hold places of importance in the industrial world. Of the three types of inkjet technologies—thermal, continuous, and piezoelectric—piezoelectric drop-on-demand (piezo DOD) is the most precise and versatile for industrial applications and can jet a wider variety of fluids at greater distances with accuracy and precision.

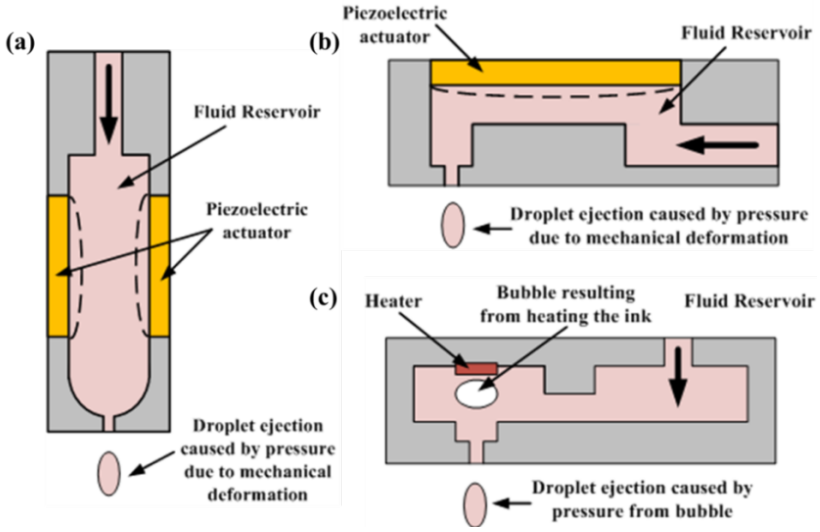


Figure 1. *Printhead technologies classified by the mode used to generate the drops (a) squeeze mode (b) bend mode of piezo inkjet and (c) bubble mode of thermal inkjet technologies.*

Relevance of Inkjet Technology today

Ink-jet printing as a fabrication technique has many attractive features. The non-contact deposition technique makes it substrate and application independent. Inkjets are also driven

digitally, under computer control, enabling the dimensional controlled deposition of inks on targeted locations. Its precision and versatility make it a deposition tool with significant benefits including but not limited to waste reduction, printing onto very large, very small, fragile, flexible or non-flat substrates, provision of higher quality output and reduction of manufacturing costs.

Inkjet technology has grown from a technique for printing two- and three-dimensional graphics production into an extremely versatile and precise technique with numerous applications in diverse realms ranging from printed circuit boards, flexible displays, optics, printed electronics and photovoltaics. This type of technology has been employed in industrial processes for adhesive coating, to deposit precise amounts of biomaterials, and to build micro- or macro-structures. In the display market, inkjet technology is used to manufacture Flat Panel Displays (FPD), Liquid Crystal Displays (LCD) and Polymer Light Emitting Diodes (PLED) [11-14]. There has been extensive research to improve their performance. Jetting of UV-curable optical polymers has allowed the production of low-cost micro-lens arrays [15,16]. The unique aspects of the technology allow the precise and uniform deposition of the micro-lenses at the end of optical fibers and other substrates. The ability of this technology for dispensing small doses of liquid makes it extremely useful in the chemical as well as biomedical market [17,18]. The high costs of these fluids make IJP with its precision and economic usage of materials an excellent dispensing tool. In the electronics market, inkjet technology is used to jet conductive silver and copper nanoparticle inks onto rigid and flexible substrates and fabricate electronic components and circuits, organic solutions to produce organic electronics and other functional fluids to produce fuel cells and batteries [19-23].

Inkjet Printing Apparatus

Presented here is the Jetlab 4 tabletop printer (MicroFab Tech, Inc.) is used to deposit the organic photovoltaic layer. The ink-jet printer consists of a piezoelectric driven inkjet head with

X-Y motorized stage which has a heating element, and a drop observation camera used to observe the formation and the pathways of the ink droplets. The schematic diagram of the printer is shown in Figure 2.

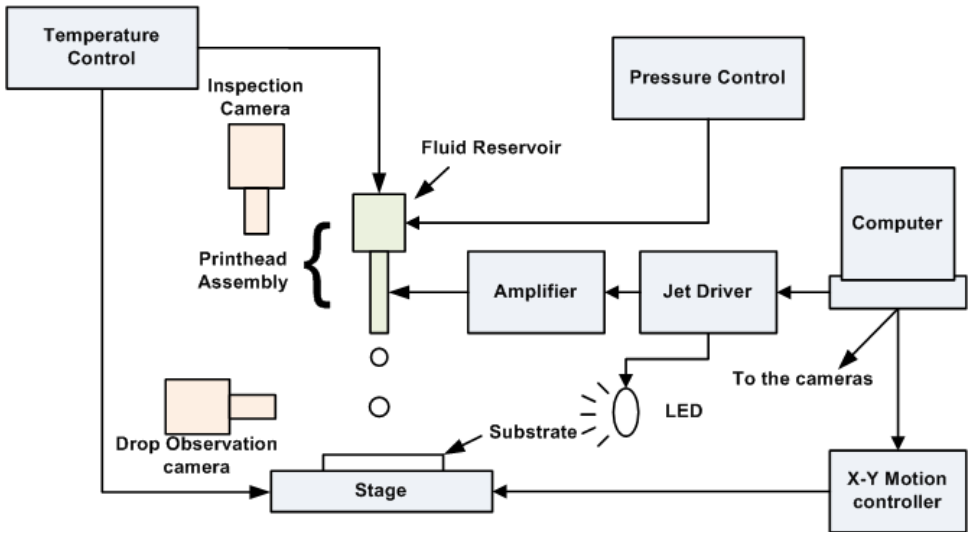


Figure 2. *Schematic diagram of the ink-jet printer*

Printhead assembly

The printhead assembly is a complex assembly of parts designed for the effective and efficient drop control. Throughout this work polymer blend deposition is carried out using a single jet piezo-electrically actuated MJ-AL-01 jetting device suited for dispensing droplets of aqueous and solvent-based fluids at up to 50°C (Figure 3). Fluids with viscosity less than 20 cP and surface tension in the range 20-70 dynes/cm with pH from 2 to 11 can be dispensed. The viscosity and surface tension of CB is 0.80 cP and 33.28 dynes/cm at 20°C and it falls within the dispensing range.

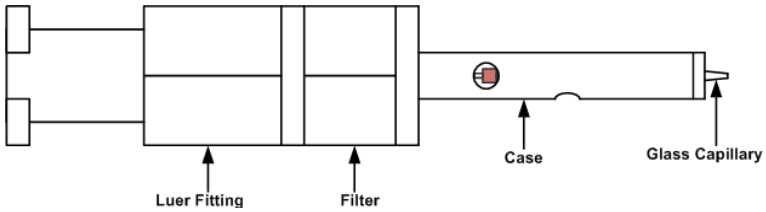
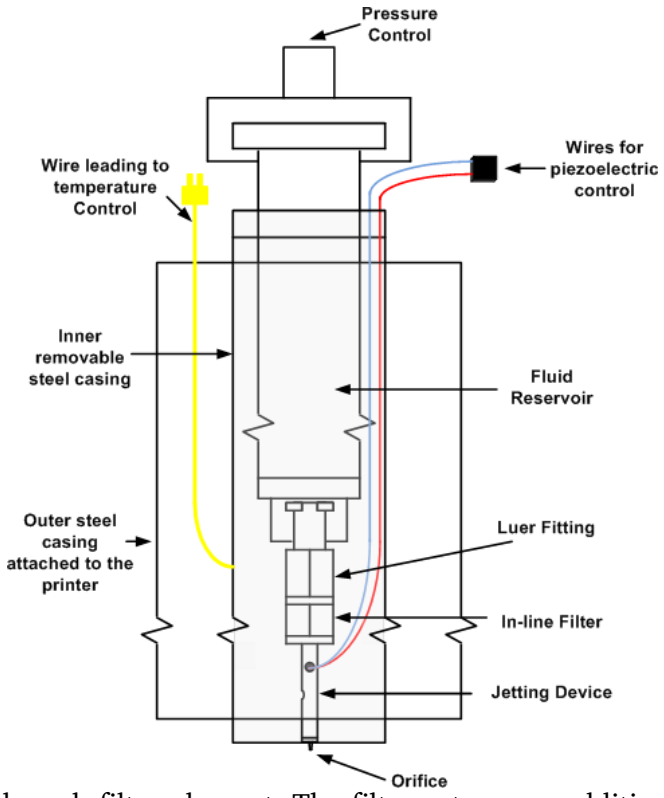


Figure 3. *Diagram of the MJ-AL-01 Jetting device*

The MJ-AL-01 jetting device consists of a small glass capillary with piezoelectric elements epoxied around the circumference of the tube. The glass capillary ends in the nozzle orifice with a diameter of 80 μm and is cased in a stainless-steel housing protected by insulating filler which is also resistant to solvents. The tip of the orifice extends from the casing, allowing visualization of drop formation or contaminants, if present. During the operation of the device, the fluid only wets stainless steel or glass surfaces, making MJ-A devices extremely robust to aggressive fluids. The glass capillary is attached to a filter with an inline removable filter with



a 5 μm stainless steel mesh filter element. The filter acts as an additional safeguard against unwanted particles which might clog the nozzle. A female luer fitting attaches the filter to the reservoir.

Figure 4. *Printhead assembly configuration diagram*

The printhead assembly consists of the dispensing device, the ink reservoir, filters, heating elements and connections to the heating, pneumatic and electronics controller

(JetDrive III) (Figure 4). The 2.5 mL capacity polypropylene reservoir attaches directly to the dispensing device and maintains the liquid at the set temperature with the help of the heating elements and a thermocouple based temperature regulator. Accurate pressure control is crucial for providing suitable printing conditions. Typically, a slight negative pressure is maintained to prevent dripping of the fluid from the tip although care is always taken so that the pressure does not cause the fluid to get backed up into the reservoir.

X-Y and Z Stages

The device can create patterns over a total printable area of 160 X 120 mm^2. The X-Y stages are equipped with linear encoders used for position maintenance. The positioning accuracies are $\pm 10\,\mu$m, with a repeatability of about $\pm 2\,\mu$m. The Z stage controls the printhead height. The X-Y stage is fitted with a heater and the temperature of the platen can be adjusted up to 150°C. The stage also has vacuum ports for the steady positioning of the substrate.

Optics subsystem

The horizontal drop observation camera is used to observe the formation and the pathways of droplets in flight. As the drop formation is periodic due to the waveform of the ac signal driving the piezoelectric transducer, a stroboscopic method is used to visualize the phenomenon. This is achieved by using a pulsed LED illuminating the tip of the nozzle in sync with the main output ac signal for drop generation. In other words, the strobe frequency is the same as the drop repetition rate. A strobe delay of varying duration is applied to the LED pulse wave in order to observe the pathway of the drops at various instants. The delay changes the relative timing of the strobe pulse to the main pulse. Every stage of the drop formation and the impact of changing various parameters of the waveform on it can be observed by adjusting the strobe delay. The inspection camera is oriented vertically and is used to inspect printed patterns.

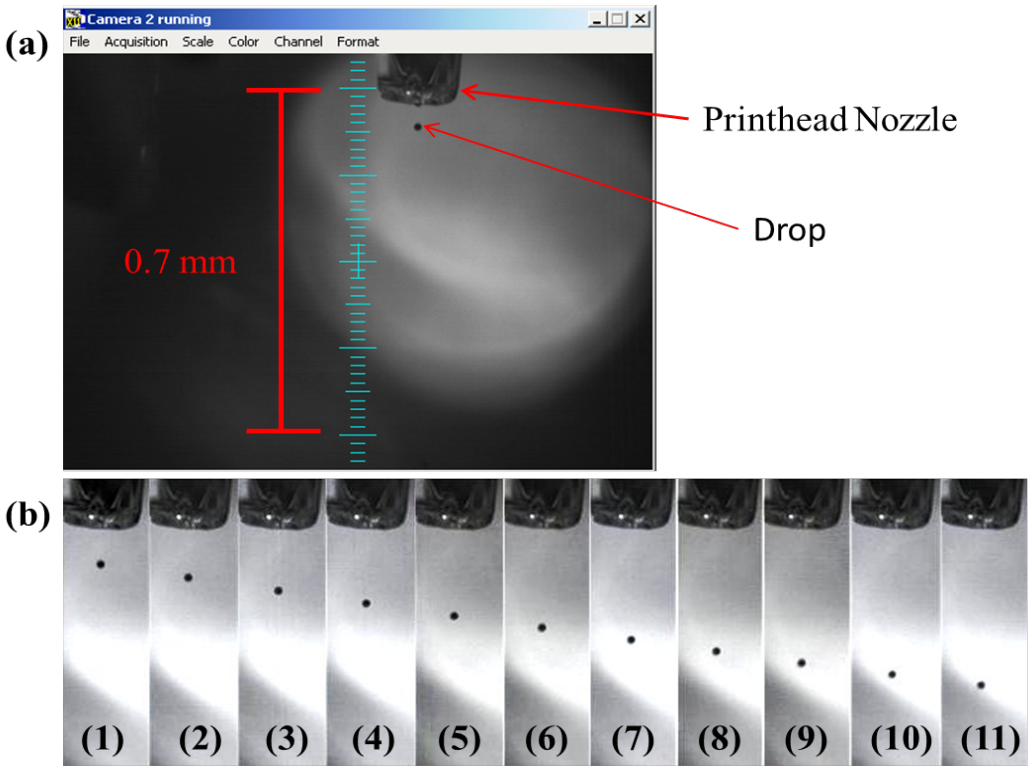


Figure 5. *(a) Close-up view of drop formation with the jetting device tip in view of the horizontal camera (b) Sequence of snapshots at a time interval 100μs of showing the pathway of a drop. The leftmost image corresponds in time to the start of the pulse (300 μs), and the last one matches approximately fall in the pulse at 1300 μs. Printing was done using isopropanol.*

Printing Principles

The drop ejection process starts when the fluid reservoir of the print head is subjected to an applied external voltage pulse, causing it to contract and reduce in volume. This volumetric change causes a sudden compression of the fluid creating an acoustic pressure wave and this overcomes the surface tension at the ink-air interface and causes the ejection of the drop from the print-head tip orifice. The jetting phenomenon has been related to the pressure wave inside the printhead by Body and Talke [24]. A description of travelling pressure waves and their behavior pertaining to propagation and reflection is reviewed below. A linear bipolar waveform and its effect of its different parts on the reservoir fluid are detailed.

Derivation of Pressure Wave Equation

In this section the derivation of wave equation is presented for reference. The wave equation

is usually represented in terms of particle displacement u(x,t) as shown in Equation (1) and it is considered as a general form of the wave equation. However, this form can also be used to directly describe the wave as pressure function P(x,t)and since the relevant parameter in our discussion is pressure, so the wave equation was derived in terms of pressure.

$$\frac{\partial^2 u}{\partial x^2} = \frac{1}{c^2}\frac{\partial^2 u}{\partial t^2} \tag{1}$$

where c is speed of sound in the ambient atmosphere.

Consider a column of air bounded by a closed surface on the right side and an air-tight piston on the other end of the long tube with a cross-sectional area A (Figure 6). The length of the original column of air can be considered as c*dt. The pressure of the air when the piston is at rest is p, the atmospheric pressure and the ambient density of air is ρ_0. When the piston starts moving with a longitudinal velocity v, the air will start getting compressed causing the pressure and density to rise and a pressure wave will be generated. After a time t, the piston would have moved forward by a distance Δv*dt, with the pressure in the enclosed region as P+ΔP and density as ρ+Δρ.

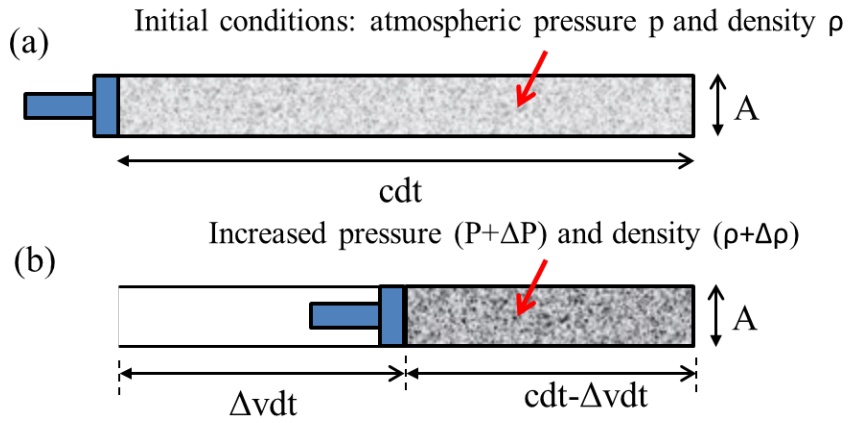


Figure 6: Representation of a bounded column of air with a snugly fit piston on the left side and a closed surface on the right. (a) Initial conditions (b) Conditions after a time dt

First, we can calculate the mass of air which will remain constant throughout the compression. Considering the situation represented in Figure 6a we get:

$$M_{\text{original}} = Acdt\rho_0 \tag{2}$$

From Figure 6b where the mass of air has been compressed into a smaller volume, we get:

$$M_{\text{compressed}} = A(cdt - \Delta v dt)(\rho_0 + \Delta\rho) \quad (3)$$

Applying the conservation of mass and equating these two equations gives us:

$$Acdt\rho_0 = A(cdt - \Delta v dt)(\rho_0 + \Delta\rho) \quad (4)$$

Rearranging the terms results in:

$$\Delta v = \frac{\Delta\rho(\rho_0 + \Delta\rho)}{c\rho_0} \quad (5)$$

In our case, we can assume that $\Delta p \ll \rho_0$ leading to:

$$\Delta v = \frac{\Delta\rho}{\rho_0} c \quad (6)$$

Equation (6) describes the relationship between the incremental change in particle velocity to the incremental change in density and it will be used later.

The relationship between the incremental changes in pressure to the incremental change in density can be derived by looking at the momentum of the air particles undergoing compression. The instantaneous momentum can be described as the total mass moved with an instantaneous velocity Δv. Thus, using Equation (2) we can write:

$$Momentum = dp = Acdt\rho_0\Delta v \quad (7)$$

We know:

$$Force = \frac{d(Momentum)}{dt} = \frac{dp}{dt} = Ac\rho_0\Delta v \quad (8)$$

So, we can now describe the instantaneous change in pressure as a result of the compressed air, by looking at the rate of change of momentum (Force) and dividing it by the area A. Thus:

$$\Delta P = \frac{F}{A} \quad (9)$$
$$\Rightarrow \Delta P = c\rho_0\Delta v$$

Using Equation (6) to substitute the incremental change in particle velocity by incremental change in density, we get:

$$\Delta P = c^2\Delta\rho \quad (10)$$

We know that the momentum equation is:

$$\frac{\partial v}{\partial t} = -\frac{1}{\rho_0}\frac{\partial P}{\partial x} \quad (11)$$

And the continuity equation is:

$$\frac{\partial \rho}{\partial t} = -\rho_0\frac{\partial v}{\partial x} \quad (12)$$

Firstly, we can differentiate Equation (11) w.r.t x and Equation (12) w.r.t t:

$$\frac{\partial^2 \rho}{\partial x \partial t} = -\frac{1}{\rho_0}\left(\frac{\partial^2 P}{\partial x^2}\right) \tag{13}$$

$$\frac{\partial^2 \rho}{\partial x \partial t} = -\frac{1}{\rho_0}\left(\frac{\partial^2 \rho}{\partial t^2}\right) \tag{14}$$

Equating Equations (13) and (14) leads to:

$$-\frac{1}{\rho_0}\left(\frac{\partial^2 P}{\partial x^2}\right) = -\frac{1}{\rho_0}\left(\frac{\partial^2 \rho}{\partial t^2}\right)$$

$$\frac{\partial^2 P}{\partial x^2} = \frac{\partial^2 \rho}{\partial t^2} \tag{15}$$

From Equation (14) we know $\Delta P = c^2 \Delta \rho$. Substituting this into Equation (15) gives the desired form of the wave equation. Thus:

$$\frac{\partial^2 P}{\partial x^2} = \frac{1}{c^2}\left(\frac{\partial^2 P}{\partial t^2}\right) \tag{16}$$

This is the pressure wave equation.

d'Alembert's solution of the wave equation

The method of d'Alembert provides a solution to the one-dimensional wave equation that models the vibrations of a string:

$$\frac{\partial^2 P}{\partial x^2} = \frac{1}{c^2}\left(\frac{\partial^2 P}{\partial t^2}\right) \tag{17}$$

The general solution can be obtained by introducing new variables ξ and η such that they satisfy the linear transformation

$$\xi = x + ct \tag{18}$$

$$\eta = x - ct \tag{19}$$

From the chain rule, we obtain:

$$\frac{\partial}{\partial x} = \frac{\partial}{\partial \xi} + \frac{\partial}{\partial \eta} \tag{20}$$

$$\frac{\partial}{\partial t} = c\frac{\partial}{\partial \xi} - c\frac{\partial}{\partial \eta} \tag{21}$$

Using Equations (20) and (21) to compute second derivatives:

$$\frac{\partial^2 P}{\partial x^2} = \frac{\partial}{\partial x}\left(\frac{\partial P}{\partial x}\right)$$

$$\frac{\partial^2 P}{\partial x^2} = \frac{\partial^2 P}{\partial \xi^2} + 2\frac{\partial^2 P}{\partial \xi \partial \eta} + \frac{\partial^2 P}{\partial \eta^2} \tag{22}$$

And similarly, we get

$$\frac{\partial^2 P}{\partial t^2} = \frac{\partial}{\partial t}\left(\frac{\partial P}{\partial t}\right)$$

$$\frac{\partial^2 P}{\partial t^2} = c^2 \frac{\partial^2 P}{\partial \xi^2} - 2c^2 \frac{\partial^2 P}{\partial \xi \partial \eta} + c^2 \frac{\partial^2 P}{\partial \eta^2} \quad (23)$$

So, substituting the respective values in Equation (17) gives us:

$$\frac{\partial^2 P}{\partial \xi \partial \eta} = 0 \quad (24)$$

This equation can be solved by direct integration. First integrating w.r.t.ξ gives us,

$$\int \frac{\partial^2 P}{\partial \xi \partial \eta} d\xi = \frac{\partial P}{\partial \eta} = f(\eta) \quad (25)$$

where const(η) is an arbitrary function of η. Then integrate w.r.t. η to obtain,

$$P(\xi, \eta) = f(\xi) + g(\eta) \quad (26)$$

where f is an arbitrary function of ξ and $g = \int const(\eta)\, d\eta$
Finally replacing the values of ξ and η from Equations (18) and (19) we get,

$$P(x, t) = f(x - ct) + g(x + ct) \quad (27)$$

This solution can be interpreted as two pressure waves moving in opposite directions along the x-axis with f(x-ct) representing a right travelling wave and g(x+ct) a left travelling wave with a constant velocity c. The general solution can be used to derive the d'Alembert solution of an initial value problem for waves in a tube of infinite length.

Exact Solution using Initial Conditions

The initial pressure distribution and the initial rate of pressure are defined by the parameters $\varphi(x)$ and $\theta(x)$, respectively. The equations defining the initial conditions are

$$P(x, 0) = \varphi(x) \quad (28)$$

$$\frac{\partial P}{\partial t}(x, 0) = \theta(x) \quad (29)$$

From Equations (27), (28) and (29) we get:

$$P(x, 0) = f(x) + g(x) = \varphi(x) \quad (30)$$

$$\frac{\partial P}{\partial t}(x, 0) = -cf'(x) + cg'(x) = \theta(x) \quad (31)$$

From Equations (30) and (31) we get:

$$cf(x) + cg(x) = c\varphi(x) \quad (32)$$

$$-cf(x) + cg(x) = \int_{x_0}^{x} \theta(s)\, ds + c_1 \quad (33)$$

Adding Equations (32) and (33) gives:

$$2cg(x) = c\varphi(x) + \int_{x_0}^{x} \theta(s)\, ds + c_1 \quad (34)$$

Rearranging Equation (34):

$$g(x) = \frac{1}{2}\varphi(x) + \frac{1}{2c}\int_{x_0}^{x} \theta(s)\, ds + c_1 \quad (35)$$

Changing variables from x→x+ct:

$$g(x + ct) = \frac{1}{2}\varphi(x + ct) + \frac{1}{2c}\int_{x_0}^{x+ct} \theta(s)\, ds + c_1 \tag{36}$$

Rearranging Equation (32)

$$2cf(x) = 2c\varphi(x) - 2cg(x)$$

$$\Rightarrow f(x) = \frac{1}{2}\varphi(x) - \frac{1}{2c}\int_{x_0}^{x} \theta(s)\, ds - c_1 \tag{37}$$

Changing variables from $x \rightarrow x - ct$:

$$\Rightarrow f(x - ct) = \frac{1}{2}\varphi(x - ct) - \frac{1}{2c}\int_{x_0}^{x-ct} \theta(s)\, ds - c_1 \tag{38}$$

From Equation (27)

$$P(x,t) = f(x - ct) + g(x + ct)$$

$$\Rightarrow P(x,t) = \frac{1}{2}[\varphi(x + ct) + \varphi(x - ct)] + \frac{1}{2c}\int_{x-ct}^{x+ct} \theta(s)\, ds \tag{39}$$

Consider the case of an infinite tube in which the initial rate of pressure $\theta(x)$ is zero. The initial conditions can then be represented by the following equation.

$$P(x,0) = \varphi(x);\ \ \frac{\partial P}{\partial t}(x,0) = \theta(x) = 0 \tag{40}$$

Using these relations in Equation (39) gives us the exact solution which is,

$$P(x,t) = \frac{1}{2}(\varphi(x - ct) + \varphi(x + ct)) \tag{41}$$

The Equations (40) and (41) describes the initial and subsequent behavior of the pressure wave, respectively. Equation (41) can be interpreted as two pressure waves with constant velocity c propagating in opposite directions along the x-axis. Figure 7 illustrates the process of division and propagation of the pressure distribution in an infinitely long tube.

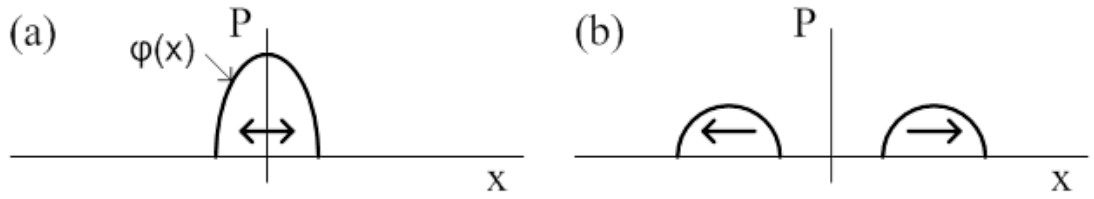


Figure 7: Illustration of (a) Initial pressure distribution $\phi(x)$ and (b) division and propagation of a pressure wave

Calculation of acoustic stress

One of the equations required is the relationship between the pressure and the rate of change of displacement with distance. Consider a tube of cross-sectional area A in which a longitudinal wave is propagating along the tube. Let C and D be two planes at distances x and

x+δx, as measured from an arbitrary origin which is constant for both (Figure 8). After a certain amount of time has elapsed, let the instantaneous positions of these planes be C' and D', respectively. If the displacement of C is y (along the x-axis), the rate of change of displacement with distance is $\frac{dy}{dx}$. The new positions of the planes will be (x+y) and $x + \delta x + y + \frac{dy}{dx}\delta x$, respectively.

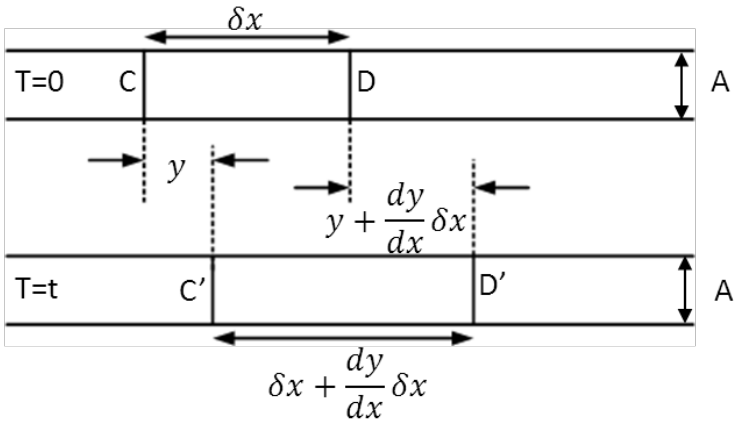


Figure 8: Initial positions of two planes of the propagating wave in a tube (b) their instantaneous position at time t.

The change is volume will be given by

$$\Delta V = V_{\text{final}} - V_{\text{initial}}$$

$$\Rightarrow \Delta V = A\left(\delta x + y + \left(\frac{\partial y}{\partial x}\right)\delta x - y\right) - A\delta x$$

$$\Rightarrow \Delta V = A\delta x + A\left(\frac{\partial y}{\partial x}\right)\delta x - A\delta x$$

$$\Rightarrow \Delta V = A\delta x\left(\frac{\partial y}{\partial x}\right) \tag{42}$$

Volume strain:

$$\frac{\Delta V}{V} = \frac{A\delta x\left(\frac{\partial y}{\partial x}\right)}{A\delta x} = \frac{\partial y}{\partial x} \tag{43}$$

Volume stress which gives acoustic pressure P will thus be

$$Volume\ Stress = P = -K * Volume\ Strain \tag{44}$$

$$P = -K\frac{\partial y}{\partial x} \tag{45}$$

where K is bulk modulus. The negative sign indicates that when pressure increases, the volume decreases. In the case of pressure waves we have according to the Newton-Laplace formula

$$K = \rho_0 c^2 \tag{46}$$

with c as speed of the wave and ρ_0 as ambient density. So, substituting in Equation (45) we get,

$$P = -\rho_0 c^2 \frac{\partial y}{\partial x} \tag{47}$$

Pressure wave reflections

The pressure reflection characteristics from open and closed ends are derived by imposing the boundary conditions and using the required equations.

We have particle velocity as

$$u = \frac{\partial y}{\partial t} \tag{48}$$

And, the acoustic pressure as derived in the previous section is given as

$$P = -\rho c^2 \frac{\partial y}{\partial x}$$

The general solution of the pressure wave is given by Equation (27)

$$P(x,t) = f(x - ct) + g(x + ct)$$

Now, the boundary condition on the open end consists of zero pressure at the boundary. This can be enforced by superimposing on the incident pressure wave a similar pressure wave of opposite sign travelling in the opposite direction outside the tube at the same distance from the end as the incident wave. For the pressure wave reflecting from an open end, the pressure wave will reflect back with a changed sign as shown in Figure 9.

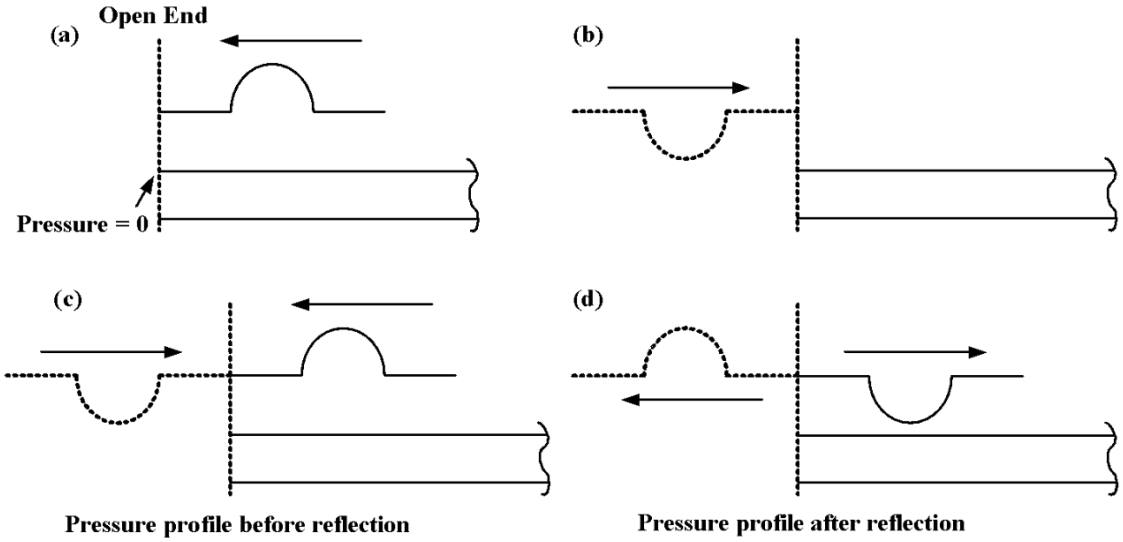


Figure 9*: (a) Incident pressure wave approaching the open end of the tube. (b) Similar pressure wave of opposite sign superimposed on the incident wave to enforce the boundary conditions. (c, d) Pressure reflections from the open end of a tube. The dotted line represents the superimposed wave.*

At the closed end, the boundary condition dictates that the velocity will zero. This can be achieved in a similar fashion as described above. The wave equation can also be expressed

in terms of displacement y and its solution will be similar to Equation (27).

$$\frac{\partial^2 y}{\partial x^2} = \frac{1}{c^2}\frac{\partial^2 y}{\partial t^2} \tag{49}$$

$$y(x,t) = f(x - ct) + g(x + ct) \tag{50}$$

If the wave is propagating in the positive x-direction i.e. $y(x,t) = f(x - ct)$, then

$$u(x,t) = -cf'(x - ct) \tag{51}$$

$$P(x,t) = -\rho_0 c^2 f'(x - ct) \tag{52}$$

This implies that velocity and pressure have the same sign.
Whereas for a wave propagating in the negative x-direction $y(x,t) = g(x + ct)$, then

$$u(x,t) = cg'(x + ct) \tag{53}$$

$$P = -\rho_0 c^2 g'(x + ct) \tag{54}$$

Therefore, we see that velocity and pressure have the opposite polarity. For the velocity wave reflecting from a closed end, the wave will reflect with a changed sign. Using Equations (51) to (54), we can plot the resultant changes in the pressure waves. A negative velocity wave travelling in the negative x-direction will correspond to a positive pressure wave in negative x-direction.

The velocity wave travelling in positive x-direction will corresponds to a pressure wave of the same sign. A more descriptive and qualitative explanation is given in the next section.

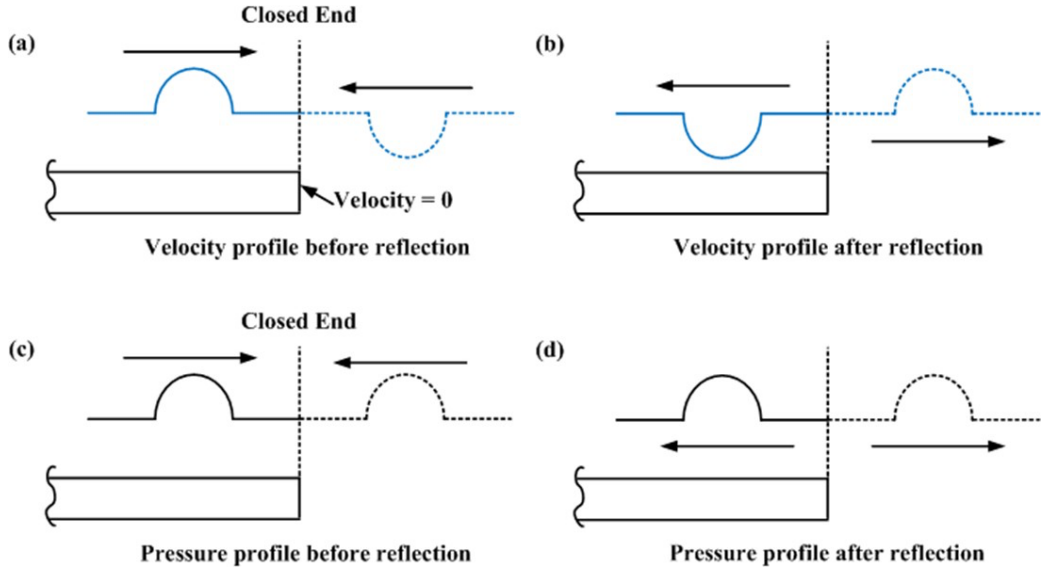


Figure 10. *Illustrations of (a, b) velocity and (c, d) pressure reflections from the closed end of a tube. The dotted line represents the superimposed wave.*

Travelling pressure waves

When a pressure wave travels along a column filled with a fluid medium such as air, plasma or liquids it produces rarefaction and compression; when it reaches the column end it is reflected. Understanding the pressure wave behavior helps us predict what occurs inside the fluid channel. Consider the simple case when a monochromatic plane sound wave is propagating down the length of a tube which has both open and closed ends. If a compression reaches the closed end, the pressure there is suddenly increased and a region of high pressure is created. The air molecules get pushed out of that region and travel along the pressure gradient in the direction opposite. Thus a compression wave gets reflected as a compression wave (Figure 11). In the same manner, a rarefaction gets reflected from the closed end of the column without getting inverted.

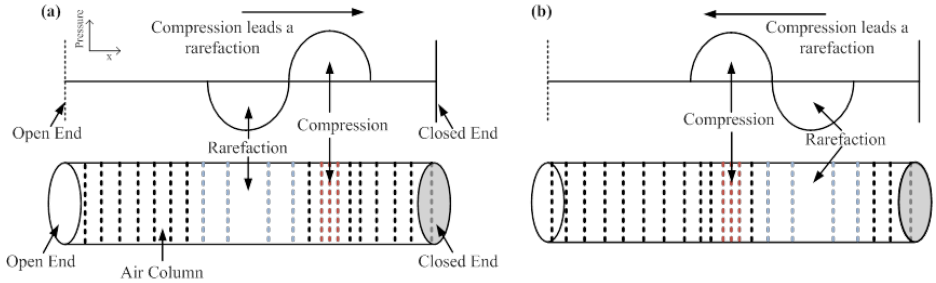


Figure 11. *Pressure wave propagation through the column (a) approaching the closed end of the column (b) returning after reflection from the closed end*

However, the process is different for the reflection from the open end of the tube. When a sound wave reaches the open end of a tube, not only is it reflected but it is also inverted. If a rarefaction reaches the open end which is at atmospheric pressure, the pressure there is suddenly reduced and a partial vacuum created. Air molecules rush in to fill this void and the pressure at the open end is restored to atmospheric pressure. The air molecules that get drawn in have inertia and they continue moving into the tube and compress the air molecules already present. A compression is created, which propagates back down the air column away from the open end. A rarefaction in the incident wave becomes a compression in the reflected wave.

Similarly, a compression in the incident wave becomes a rarefaction in the reflected wave. Figure 12 shows one cycle of a sinusoidal pressure wave travelling down an air column and being reflected at the open end.

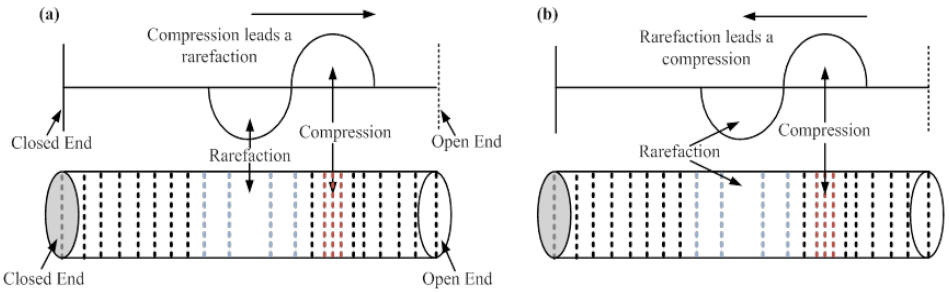


Figure 12. *Pressure wave propagation through the column (a) approaching the open end of the column (b) returning after reflection from the open end*

The propagation of the pressure wave in the fluid container follows the same principles.

Dispensing Theory

The typical voltage pulse applied to the piezoelectric actuator is a trapezoidal waveform (Figure 13). The first part of the waveform is a ramp from low to high voltage levels and results is an expansion of the cross-section of the piezo element located at the center of the ink-jet dispenser. This expansion causes the glass tube to bend outwards, and a negative pressure wave is generated which splits up and propagates in opposite directions away from the center. This expansion is maintained until the next falling step of the waveform from high to low voltage which results in contraction. The time between the expansion and contraction is referred to as the dwell time. The contraction produces a positive wave which starts to propagate in opposite directions towards both the supply and the orifice ends.

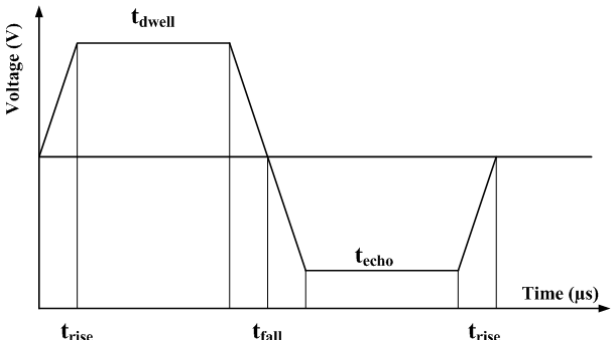


Figure 13. *Bipolar voltage waveform applied to the piezoelectric actuator.*

The boundary conditions of the ink channel can be simplified with the ink supply end being considered as an ideal open end and the jetting orifice can be modeled as an ideal closed end. This assumption is valid because the inner diameter of the reservoir is considerably larger than that of the squeeze tube of the jetting device and the nozzle opening is a small fraction of the cross-sectional area of the tube. When the traveling pressure wave reaches the supply end which it treats as an open end, it reflects with an opposite sign. On reaching the orifice of the jetting device, the pressure wave reflects without inverting as in the case of reflection from a closed end.

Figure 14 illustrates a sequence of pressure pulse propagations and reflections. Upon the initial expansion of the capillary tube caused by a positive voltage ramp at initial time (set as 0), a negative pressure wave is generated. This negative pressure wave splits into two propagating waves with half the original amplitude and they travel in opposite directions, towards the supply and orifice ends. When the pressure waves reach the ends, they reflect according to the reflection rules described above. The pressure wave reaching the orifice reflects with the same sign, but the wave reaching the supply end reflects and changes to a positive pressure wave. After time L/C, the pressure waves superimpose on each other at the center where L is the length of the dispenser and C is the speed of sound in the fluid. A negative voltage ramp applied at this instant, contracts the tube and generates a positive pressure wave. This cancels out the negative pressure wave and doubles the magnitude of the left propagating

positive wave. When this reinforced wave reaches the orifice which is a constant pressure boundary, impedance mismatch occurs and the acoustic energy is converted to kinetic energy and drop ejection occurs. Thus, the optimal pulse width is L/C and drop ejection begins after a time period of 3L/2C after the initial voltage ramp.

The residual pressure waves keep propagating in the channel and may cause unwanted drop ejections with a period of 4L/C (Figure 15). A positive voltage ramp after a period of 2L/C from initial expansion will generate a negative pressure wave which will damp out the positive contraction of the residual pressure waves. The time between the last negative contraction and this final positive expansion is referred to as the echo dwell.

In practice, the optimum dwell time is determined experimentally as the parameters L and C might be unknown. The optimized dwell time corresponds to the maximum drop velocity and the dwell time is changed till this is achieved.

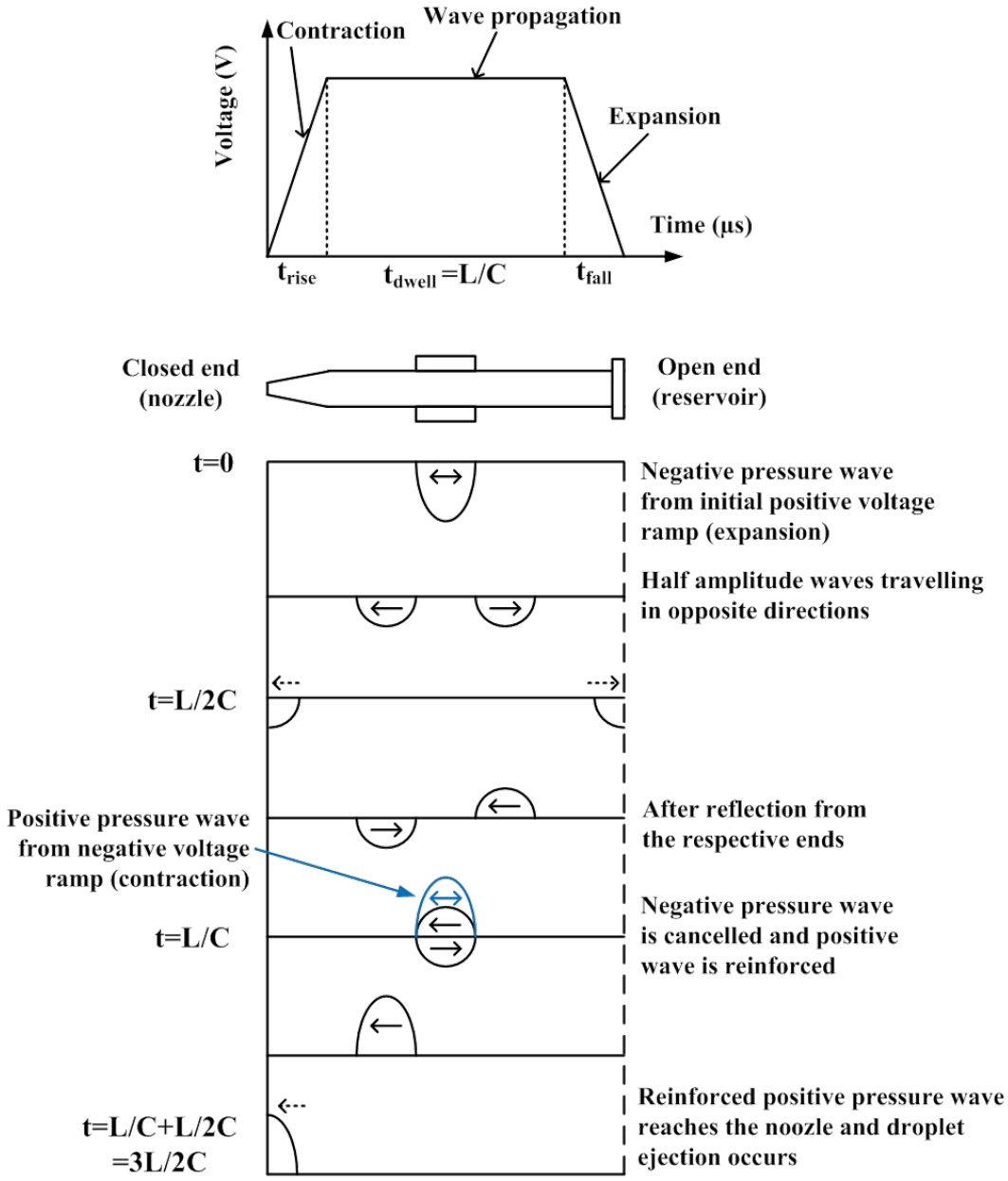


Figure 14. *Illustration of pressure wave propagation and reflections in an inkjet dispenser detailing the drop ejection process*

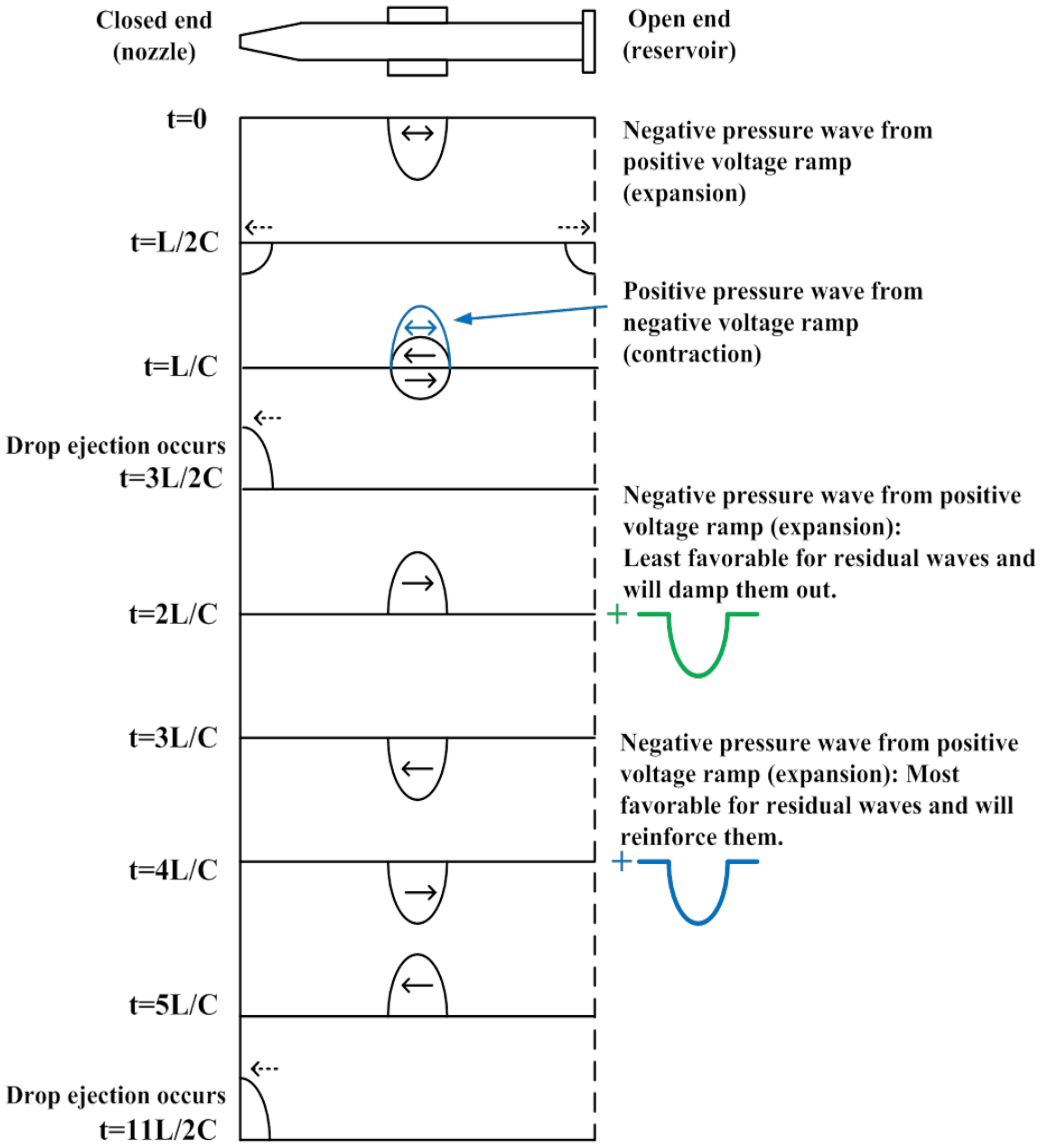


Figure 15. *Illustration of pressure wave propagation and reflections in an inkjet dispenser detailing reflections of the residual waves*

As various uses are found for organic semiconductors and their market continues to grow, inkjet printing will become more critical in the manufacture of niche electronic devices and beyond when efficiencies reach and match those of silicon, the main energy market. This work aimed to improve understanding of inkjet printing process of polymers, it was demonstrated that the print pattern, annealing conditions, substrate temperature and

evaporation rates play a vital role in the printing of organic layer for OPVs [25,26]. This suggests a careful management of these parameters is critical in the fabrication of quality organic semiconductor films [27,28]. The interplay between inkjet printing parameters and the morphology of inkjet printed films was studied using profilometry. However, the changes in the morphology with the incorporation of additives need to be investigated more and are not fully understood still [29]. To fully exploit the technique and to expertly control it for technological application a more complete knowledge base is required [12,30,31].

Conclusion

Inkjet printing as a solution dispensing tool has many attractive features due to its precise and versatile deposition technique. Inkjet printing being a non-contact deposition technique makes it substrate and application independent (when adhesions are permissible) allowing deposition on flexible and non-flat substrates of different sizes with real-time responsiveness and potentially high speeds. It allows the dimensional controlled deposition of inks on targeted locations up to micron scale accuracy. The two-dimensional patterning ability negates the need of masks and thus, an extra fabrication step. This tight control also helps in minimizing material waste. As such, the technique is favorably disposed towards integration in industrial scale production, providing cost reduction of existing components as well as opportunities for pioneering new strategies.

Acknowledgement

The authors would like to acknowledge Integricote for the funding of materials and sponsorship of the paper.

References

[1] Savart, F. (**1833**). Mémoire sur la constitution des veines liquides lancées par des orifices circulaires en mince paroi. *Ann. Chim. Phys.*, *53*, 337–386.

[2] Plateau, M. T. (**1856**). XXXVII. On the recent theories of the constitution of jets of liquid issuing from circular orifices. *Philosophical Magazine Series 4*, *12*(79), 286–297.

[3] Rayleigh, L. (**1878**). On The Instability Of Jets. *Proceedings of the London Mathematical Society*, *s1-10*(1), 4–13.

[4] Young, T. (**1805**). An Essay on the Cohesion of Fluids. *Philosophical Transactions of the Royal Society of London*, *95*, 65–87.

[5] Laplace, P. S. (**1805**). *Traite de Mechanique Celeste* (Vol. 4, Supplements au Livre X). Courier.

[6] Sweet, R. G. (**1965**). High Frequency Recording with Electrostatically Deflected Ink Jets. *Review of Scientific Instruments*, *36*(2), 131–136.

[7] Hansell, C. W. (**1950**). *Jet sprayer actuated by supersonic waves* (U.S. Patent No. 2,512,743). RCA Corp.

[8] Zoltan, S. I. (**1972**). *PULSED DROPLET EJECTING SYSTEM* (U.S. Patent No. 3,683,212).

[9] Stemme. (**1973**). *ARRANGEMENT OF WRITING MECHANISMS FOR WRITING ON PAPER WITH A COLORED LIQUID* (U.S. Patent No. 3,747,120).

[10] Kyser, E. L. (**1976**). *Method and apparatus for recording with writing fluids and drop projection means therefor* (U.S. Patent No. 3,946,398).

[11] Koo, H.-S., Chen, M., & Pan, P.-C. (**2006**). LCD-based color filter films fabricated by a pigment-based colorant photo resist inks and printing technology. *Thin Solid Films*, *515*(3), 896–901.

[12] de Gans, B. J., Duineveld, P. C., & Schubert, U. S. (**2004**). Inkjet Printing of Polymers: State of the Art and Future Developments. *Advanced Materials*, *16*(3), 203–213.

[13] Koo, H. S., et al. (**2006**). Fabrication and chromatic characteristics of the greenish LCD colour-filter layer with nano-particle ink using inkjet printing technique. *Displays*, *27*(3), 124–129.

[14] Fisslthaler, E., et al. (**2008**). Inkjet printed polymer light-emitting devices fabricated by thermal embedding of semiconducting polymer nanospheres in an inert matrix. *Applied Physics Letters*, *92*(18), 183305.

[15] Tien, C.-H., Hung, C.-H., & Yu, T.-H. (**2009**). Microlens Arrays by Direct-Writing Inkjet Print for LCD Backlighting Applications. *Journal of Display Technology*, *5*(5), 147–151.

[16] MacFarlane, D. L., et al. (**1994**). Microjet fabrication of microlens arrays. *IEEE Photonics*

Technology Letters, *6*(9), 1112–1114.

[17] Goldmann, T., & Gonzalez, J. S. (**2000**). DNA-printing: utilization of a standard inkjet printer for the transfer of nucleic acids to solid supports. *Journal of Biochemical and Biophysical Methods*, *42*(3), 105–110.

[18] Lemmo, A. V., Rose, D. J., & Tisone, T. C. (**1998**). Inkjet dispensing technology: applications in drug discovery. *Current Opinion in Biotechnology*, *9*(6), 615–617.

[19] Li, Y., et al. (**2007**). Integration of sensors and inkjet-printed RFID tags on paper-based substrates for UHF "Cognitive Intelligence" applications. In *Antennas and Propagation Society International Symposium, 2007 IEEE*.

[20] Pech, D., et al. (**2010**). Elaboration of a microstructured inkjet-printed carbon electrochemical capacitor. *Journal of Power Sources*, *195*(4), 1266–1269.

[21] Kim, H. S., et al. (**2009**). Inkjet printed electronics for multifunctional composite structure. *Composites Science and Technology*, *69*(7–8), 1256–1264.

[22] Taylor, A. D., et al. (**2007**). Inkjet printing of carbon supported platinum 3-D catalyst layers for use in fuel cells. *Journal of Power Sources*, *171*(1), 101–106.

[23] Sirringhaus, H., et al. (**2000**). High-Resolution Inkjet Printing of All-Polymer Transistor Circuits. *Science*, *290*(5499), 2123–2126.

[24] Bogy, D. B., & Talke, F. E. (**1984**). EXPERIMENTAL AND THEORETICAL-STUDY OF WAVE-PROPAGATION PHENOMENA IN DROP-ON-DEMAND INK JET DEVICES. *Ibm Journal of Research and Development*, *28*(3), 314–321.

[25] Haldar, A., Yambem, S. D., Liao, K.-S., Dillon, S. P., Barron, A. R., & Curran, S. A. (**2010**). Organic photovoltaics using thin gold film as an alternative anode to Indium Tin Oxide. *Proceedings of the 35th IEEE Photovoltaics Specialists Conference*, Jun 20–25, Hawaii, USA.

[26] Haldar, A., Yambem, S. D., Liao, K.-S., Alley, N. J., Dillon, E. P., Barron, A. R., & Curran, S. A. (**2011**). Organic photovoltaics using thin gold film as an alternative anode to Indium Tin Oxide. *Thin Solid Films*, *519*, 6169–6173.

[27] Haldar, A., Liao, K.-S., & Curran, S. A. (**2012**). Effect of printing parameters and annealing on organic photovoltaics performance. *Journal of Materials Research*, *27*(16), 2079–2087.

[28] Haldar, A., Liao, K.-S., & Curran, S. A. (**2012**). The effect of printing parameters and annealing on organic photovoltaic's performance. Accepted by *Journal of Materials Research*.

[29] Haldar, A., Liao, K.-S., & Curran, S. A. (**2014**). Fabrication of ink-jet printed organic photovoltaics on flexible Ag electrode with additives. *Solar Energy Materials & Solar Cells*, *125*, 283–290.

[30] Kawase, T., et al. (**2003**). Inkjet printing of polymer thin film transistors. *Thin Solid Films*, *438-439*, 279–287.

[31] Singh, M., et al. (**2010**). Inkjet Printing-Process and Its Applications. *Advanced Materials*, *22*(6), 673–685.